DOI: 10.13009/EUCASS2023-748
Aerospace Europe Conference 2023 – 10TH EUCASS – 9TH CEAS

Optimized Active Flow Separation Control in the Slat-cut Region Using Low Duty Cycle Pulsed Jets

F. Bahri , S. Qiangqiang, M Jabbal, R. Jefferson-Loveday
University of Nottingham, University Park, NG7 2RD, United Kingdom

W. Stryczniewicz, W. Stalewski
ŁRN, Institute of Aviation, al. Krakowska 110/114, 02-256 Warsaw, Poland

B. Stefes, A. Buescher
Airbus Operations GmbH, Bremen, Germany

The design of Ultra High Bypass Ratio (UHBR) engines requires a large leading-edge slat cut-out to maintain clearance between the nacelle and the ground. During the take-off and landing, when the slats are deployed, the maximum lift coefficient is undermined not only by the missing slat and the geometry changes in the cut-out area, but it is also noticeably affected by a local separation observed at the back of the cut-out at high angles of attack. The effect of active flow control (AFC) by pulsed jets on a separated flow developed at high angle of attack of a DLR-F15 wing model is investigated experimentally. A swept wing model of a chord of 0.34 m and length of 3.33 chords, in a landing configuration, is considered. A built-in Pulsed Jet Actuator (PJA) module enables 88 nozzles controlled by solenoid valves embedded in the wing model to control the flow separation. The PJA module is designed to control each valve independently in duty cycle, frequency, and starting time relative to the first valve. Flow visualisation, as well as force measurements and pressure distribution, are conducted to examine the effect of the AFC on the separation developed at a high angle of attack of the wing model. It is shown that the lift coefficient is governed mainly by the dimensionless frequency F+ of the pulsing, the pulsing duty cycle DC, and the velocity ratio Vr. The impact of DC and the dimensionless frequency F^+ on the lift improvement are examined. Also, it is found that reducing DC and F^+ of the pulses are remarkably improving the lift coefficient. In addition, the effect of the momentum coefficient C_μ on the stall angle is analysed

Nomenclature

$Aref$	=	reference area
C	=	chord length
C_l	=	lift coefficient
C_μ	=	momentum coefficient
C_p	=	pressure coefficient
DC	=	duty-cycle
F^+	=	non-dimensional frequency
f	=	forcing frequency
$\dot{m}$	=	mass-flow-rate
p, p_∞	=	pressure, freestream pressure
t_{active}	=	active pulse time
t_{pulse}	=	total time of a pulse
Δt^*	=	dimensionless time step
u_{jet}	=	jet velocity
U, U_∞	=	velocity, freestream velocity
Vr	=	velocity ratio
Λ	=	swept angle
μ	=	dynamic viscosity
ρ, ρ_∞	=	density, freestream density

DOI: 10.13009/EUCASS2023-748

Introduction

Active Separation Control (ASC) technique has been heavily investigated mainly to eliminate the separation. Two distinct approaches were considered for ASC to suppress a local flow separation. Firstly, suppressing local separation by adding only momentum i.e., zero net-mass-flux to the boundary layer. This approach was mostly conceived as a series of synthetics-jets or plasma actuators mounted on the surface at a specific location [1],[2],[3] and [4]. Secondly, adding net-mass flux and momentum to the boundary layer from an external source to prevent the separation. This methodology was recently realised by the pulsed jet mounted on the surface at the desired position. The geometry of the jet (size, shape as well its inclination to the surface) is central in succeeding in better control.

In modern aircraft, Ultra High Bypass Ratio (UHBR) engines are now more commonly used in civil aviation because they have demonstrated their commercial and environmental advantages by producing high thrust at lower consumption [5]. At present, the integration of the UHBR engines beneath the wings of the actual design and in the future development will persist for some time. Due to the relative size of the UHBR engines, a leading-edge slat cut-out was necessary to maintain a clearance between the nacelle and the ground. The choice of cutting a slat seems more efficient than redesigning longer landing [6].

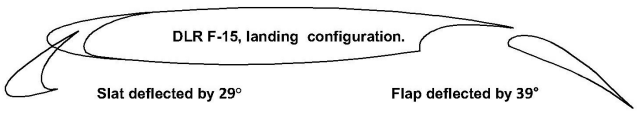

Fig. 1 Schematic view of the W-T model.

In the slat design, it was found that the maximum lift and stall angle are not only compromised by the missing slat cut-out and geometrical changes in the leading-edge, but also by a local separation that appears on the inboard side and the back of the cut-out at high angles of attack [7] [8] [9]. In this context, on a large-scale model, ASC has been indicated, through oil flow visualisations and forces measurements, that the maximum lift coefficient could be increased by up to 5.6% and the stall incidence angle could also be delayed by up to 2.3 °degrees [10] if jets are used at a high Mach number. The basic idea behind the ASC is to increase the momentum of a boundary layer through an external source in order to boost its resistance to adverse pressure gradients. Different actuators were developed recently [11] and periodic excitation with pulsed jets using solenoid was shown to be more suitable for enhancing separation control [12]. Pulsed-jet actuators have shown great effectiveness to suppress the separation at a wide range of Reynolds number and at high angles of attack. Many investigations were carried out for pulsed jet, [13] studied the effect of the pulsed jet actuator angle on the reattachment phenomena of the separation. However,[14] described the oscillatory blowing jet on airfoils and found that the separation control is affected by the size, location, momentum, and frequency of the jet. According to a numerical simulation [15], the pulsed blowing jet on the trailing-edge flap does prevent local separation. This is probably not only due to the manipulation of frequency and amplitude of the jet, but by additionally imposing a desired duty-cycle, it will have an advantage on reducing the net-mass-flux injected into the boundary layer [16].

The ASC depends mostly on the aerodynamics of the case, the nature of the boundary layer, and the mechanism causing the separation. As a result, quantifying these descriptions is rather difficult, but few essential parameters are commonly used to determine the control such as air jet velocity, jet frequency actuation, and momentum flux added to the boundary layer. The velocity ratio Vr is one parameter affecting the separation control.

$$Vr = \frac{u_{jet}}{U_\infty} \tag{1}$$

Where u_{jet} is the mean velocity of the jet generated by the PJA and U_∞ is free-stream velocity. The frequency of the actuation is defined as a non-dimensional frequency in analogy with Strouhal number.

$$F^+ = \frac{f.C}{U_\infty} \tag{2}$$

The dimensionless frequency F^+ defines the number of pulses produced by the PJA system, as the flow crosses the whole chord length C of the model. The pulsing frequency f, is measured in Hz. The duty-cycle DC is the ratio of the active pulse to the total time of the pulse, defined as:

$$DC = \frac{t_{active}}{t_{pulse}} \tag{3}$$

The other parameter describing the control is the blowing momentum coefficient C_μ which quantifies the amount of air-mass-flux brought into the boundary layer.

$$C_\mu = \frac{\dot{m}.u_j}{q.A_{ref}} \tag{4}$$

Where, $\dot{m}$ is the mass flow, q is the free-stream dynamic pressure and A_{ref} is the reference area. In order to control the separation, [9] found that on a real-scale wind tunnel model, the pulsed jet actuators can completely eliminate the separation observed behind the slat cut-out in the pylon-wing design. On the other hand, according to [17] and [18], a PJA system still requires a significant amount of energy to be installed in a civil aircraft. In this context, PJA's with variable duty-cycles would be a solution to address these issues since it would be able to regulate the quantity of momentum supplied into the boundary layer.

DOI: 10.13009/EUCASS2023-748

Experiment

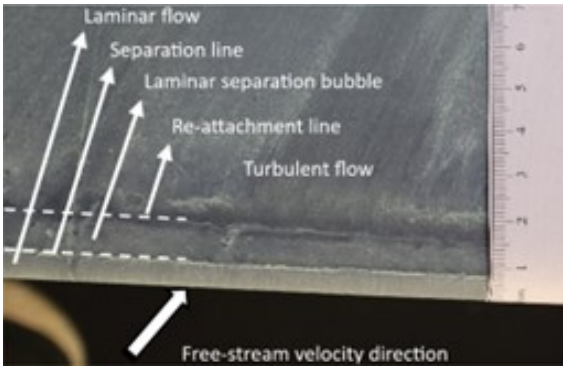

Fig. 2 Oil visualisation of the laminar bubble without tripping device, $\alpha = 5°$, Re=10^6

Fig. 3 DLR F-15 model mounted in the wind tunnel.

A. Wind Tunnel model.

The experiments were performed in Donald Campbell wind tunnel at the University of Nottingham, using a state-of-the-art wing model. The parallel three-elements $DLR-F15$ model wing precisely machined from Aluminium, has a constant chord C of 0.34 m, a length of one metre, and swept at $\Lambda = 28°$. The model is mounted vertically in the test section of the wind tunnel to a force balance as shown in Figure 3. The main element and the flap of the model are equipped with 64 static pressure taps covering both the upper and lower sides. Furthermore, an identical replica model which was realised by 3D-printing, made from PLA and mounted in aluminium spar, is dedicated solely to the flow visualisations. Both models are maintained at a landing configuration, where maximum lift coefficient is expected with the slat deflected at 29° and the flap at 39° Figure 1. In order to avoid the development of the laminar separation bubble on the smooth surface of the model, a campaign of surface oil visualisation was carried out with and without laminar-turbulent stripes such as thin trip wire and several rough tapes are used. A tape of 100-micron roughness and 20 mm width flash-mounted (no thickness) on the leading edge and centred on the stagnation line is found to be the most effective Figure 2.

B. Pulsed Jet Actuator system (PJA).

The pulse jet actuators (PJA) system consists of a module compromising the leading-edge, a pressure chamber, solenoid valves, and nozzles. The volume of the pressure chamber is considered to maintain a homogeneous pressure distribution to the inlet of the valves. 44 solenoid valves (Festo-MHJ10, fast-switching valves) control 88 nozzles, where each valve controls two adjacent nozzles. The nozzles are distributed equally through the length of the PJA and are located at 10% of the wing chord C [8]. The nozzles are of a rectangular shape of 3.5 mm × 0.43 mm and are equally spaced at 3.5 mm from each other. In addition, they are inclined at 30° relative to the wall. The projection of the width of the nozzles at the surface is still well less than 1 mm [19]Schlosser et al [21]. The manufacturing and assembly of the PJA are well detailed in [20]. A Kulite pressure transducer is mounted in one nozzle to allow measurement of the static pressure at the exit of the nozzle. A detailed schematic of a section from the wing model is shown in Figure 4.

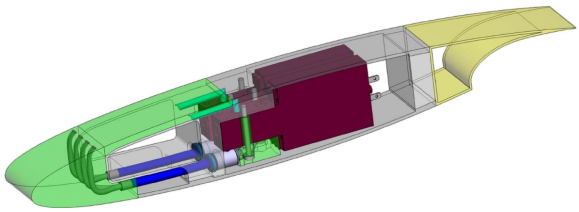

Fig. 4 Description of the PJA system, with valves position and nozzles orientation

C. Flow visualisation.

A campaign of surface oil and smoke flow visualisations on the replica model at a Reynolds number of 10^6 revealed the angle of attack that provokes the separation behind the slat cut-out. As shown in Figure. 5, the separation starts at an angle of attack $\alpha \leq 9°$. Furthermore, smoke visualisation at lower Reynolds number Re=1.8 10^5, clearly shows the separation at an angle of attack of $\alpha = 12°$ see Figure. 6.

DOI: 10.13009/EUCASS2023-748

Fig. 5 Oil flow visualisation at $\alpha = 9°$, starting of the separation at the cut-out. Re=10^6. (flow from right to left).

The following section describes the flow with and without control and discusses it in line with lift force measurements, the pressure distribution data, and oil surface flow visualization.

Results

This paper discusses the suppression of the separation with and without pulsing jets and is supported by measurements of the lift force, the pressure distribution, and flow visualisation. In all experiments, lift and drag forces together with the pressure measurements data are taken simultaneously for each run. The wind tunnel's free-stream velocity is adjusted to cover a fixed Reynolds number of 0.7 10^6 corresponding to a free-stream Mach number of 0.09. The aim of this work is to impose to the pulsed jet different frequencies and different duty-cycles with a constant velocity ratio to control the separation developed behind a slat ct-out of a DLR F-15 wing model. Several work has been done to tackle the separation by finding the optimum frequency and velocity ratio of the jet excitation. [4] suggested that the reattachment to a straight surface, the most effective frequency to prevent separated flow could be around $3 < F^+ < 4$. Also, [21] find in his numerical simulation that the flow separation on a large scale-model engine-wing configuration at high velocity ratio Vr could well be suppressed by pulsed actuation. Moreover, this simulation shows that there is a little impact on the variation of the frequency varying between $1.28 < F^+ < 6.38$ for a pulsing jets with 50% duty cycle. In a recent work, [12] studied the influences of single-pulse jet, the pulse delay and the influence of the pulse duration. In that work, a range of much lower frequencies was covered ($0.3 < F^+ < 2.3$).

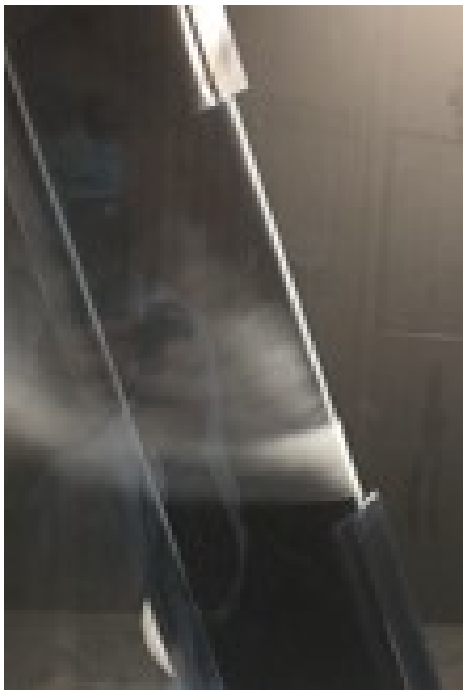

Fig. 6 Flow separation visualised by smoke at $\alpha = 12°$ and Re=1.8 10^5.

In this study, only two sets of experiments are presented. Imposing two pulsing frequencies $F^+ = 0.5$ and $F^+ = 2.0$, and covering the range of duty cycle of 20%, 30%, 40%, 50%, 60%, and 70% along with the baselines of continuous blowing and no control.

Figure. 7 presents the lift coefficient characteristics versus the angle of attack for different duty-cycle cases with the frequencies $F^+ = 0.5$ shown in Figure. 7a, and $F^+ = 2.0$ shown in Figure. 7b respectively. The baseline measurements, represented by the lower curve without control ($DC = 0\%$, valves all-time close) and the upper curve with continuous blowing ($DC = 100\%$, valves all-time open), are independent of frequency and duty-cycle. Figure. 7a further shows how continuous blowing causes the maximum lift coefficient C_{lmax2} to increase by about 17.1% in comparison to no control C_{lmax1}. It is important to notice that the C_{lmax2} evolved at the angle of attack α_2, is only about one deg. further. The gain in maximum lift, when continuously blowing ($DC = 100\%$) did not seems benefit from any remarkable delay in the stall angle with regard to the no control case ($DC = 0\%$).

In Figure. 7a, the linear branch of the lift coefficient curves where the incidences $\alpha \leq \alpha_0$ shows that the increase of the duty-cycle moved the lift coefficient toward the upper baseline ($DC = 100\%$) when the frequency is $F^+ = 0.5$. Meanwhile, the same linear branch in Figure 7b shows that the increase of the duty-cycle kept the lift coefficient near the lower baseline ($DC = 0\%$) when the frequency is $F^+ = 2.0$.

Additionally, the increase of the lift coefficient in the linear branch $\alpha \leq \alpha_0$ in Figure. 7a and Figure. 7b, seems to be relatively small compared to the change of the maximum lift at higher angle of attack. This might be the effect of pulsing into a boundary layer when separation has not yet developed. Oil visualisation, Figure. 5 confirms that the flow start to separate at $\alpha = 9°$ and fully separated in Figure. 6 when $\alpha = 12°$.

DOI: 10.13009/EUCASS2023-748

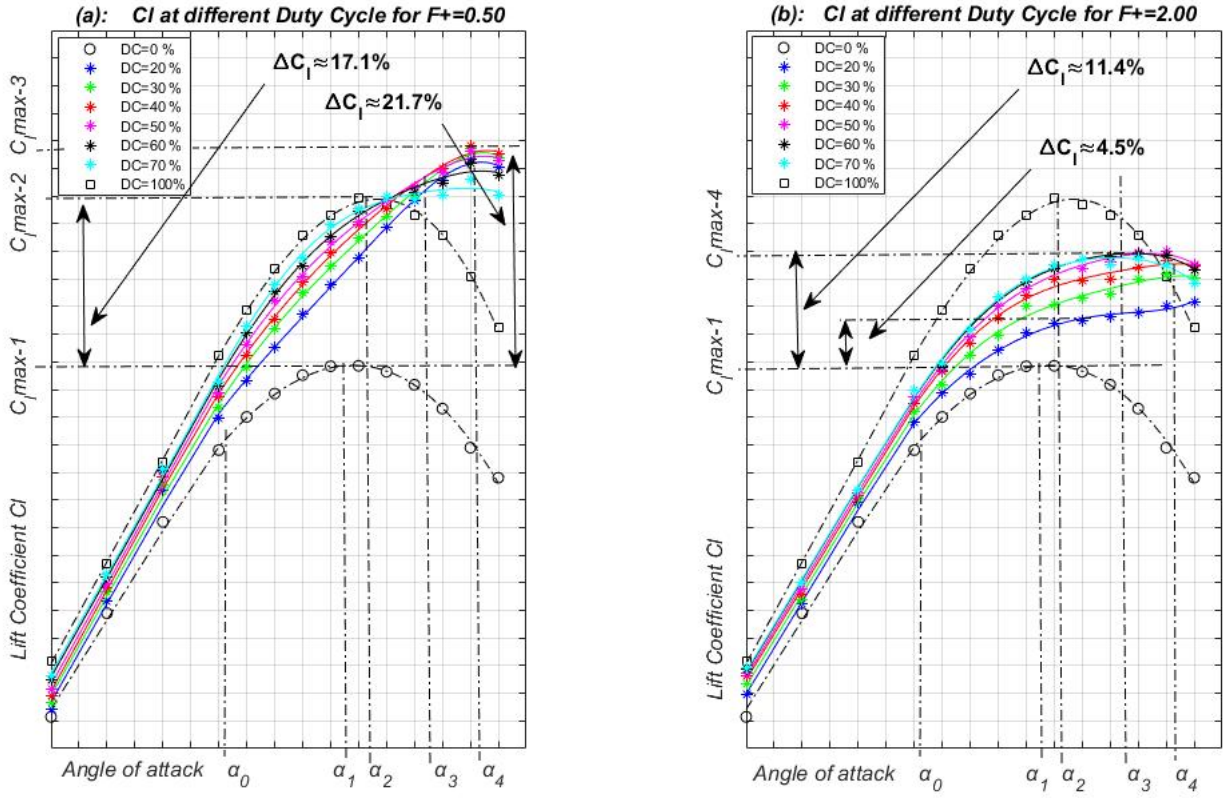

Fig. 7 Lift Coefficient for all DC at (a): $F^+ = 0.5$ and (b):$F^+ = 2.0$

On the other hand, it is noticeable in the region of interest $\alpha_0 < \alpha < \alpha_3$ in Figure. 7a, that the lift coefficient shows an increase gradually with the increase of the duty-cycle and did not exceed the upper baseline. At a critical angle of attack α_3, in Figure. 7a, the growth of the lift coefficient overtakes the upper baseline curve ($DC = 100\%$). Also, at a higher angle of attack $\alpha > \alpha_3$, the growth of the lift appears to be inverted. The lift coefficient of higher duty-cycle $DC = 70\%$ appears to be saturated meanwhile the lift coefficient of lower duty-cycles DC is still growing to reach a maximum at the angle of attack of α_4. The maximum lift coefficient in Figure. 7a, shows an increase of more than 21% if pulsing at low frequency $F^+ = 0.5$ compared to the no control. Moreover, pulsing at low frequency $F^+ = 0.5$, appears to delay the stall angle significantly from α_2 to α_4 by about 4°. At the highest frequency $F^+ = 2.0$ presented in Figure. 7b, the lift coefficient shows a moderate increase with the increase of the duty-cycle DC. A maximum lift increases of about 11.4% for pulsing at DC=70% and only 4.5% for pulsing at DC=20% at the incidence α_3.

Figure. 7b, also shows that the maximum lift coefficient at $F^+ = 2.0$, is blunted and less sharp compared to the lower frequency $F^+ = 0.5$. The stall angle seems to be around α_4 for higher duty-cycles DC=40%, 50%, 60%, 70% and slightly delayed $\alpha \geq \alpha_4$ for lower duty-cycles DC=20% and 30%. The interesting observation in the case of high frequency $F^+ = 2.0$ is that the maximum lift coefficient fairly maintains the same value for a range of angles of attack $\alpha_2 < \alpha < \alpha_4$.

Figure. 8, compares the lift coefficient between the two distinct frequencies $F^+ = 0.5$ and $F^+ = 2.0$ for each duty cycle along with the baseline curves of no control ($DC = 0\%$) and continuous blowing ($DC = 100\%$). Also, it shows that for the incidence $\alpha > \alpha_0$, the lift coefficient at lower frequency $F^+ = 0.5$ increases significantly and almost linearly compared to the higher frequency at the same duty-cycle. The maximum lift coefficient goes above the upper baseline of continuous blowing for the duty-cycles DC=20%, 30%, 40%, 50%, 60% and the stall angle further delayed by 4°. An interesting finding about how the lift coefficient varies with the low frequency $F^+ = 0.5$ is that, up until the critical incidence α_c, the lift exhibits a "linear-type" increase with an increase in duty cycle. Above the critical incidence α_c, high lift is obtained with lower duty-cycles. However, at higher frequency $F+ = 2.0$, the lift coefficient appears to rise parabolically and quickly flatten from the very low duty-cycles and never reaches the upper baseline of constant blowing. Also, it shows that it is encapsulated between the lower baseline "no control" and the upper baseline "continuous blowing". This observation leads to a suggestion that at a higher pulsing frequency $F^+ > 2.0$, the lift coefficient will increase as same as you move the lower baseline up towards the upper baseline by increasing the duty-cycle. Also, in the same manner, pulsing at very high frequencies $F^+ >> 2.0$ the duty-cycle will not have any effect and the control will be the same as continuous blowing.

DOI: 10.13009/EUCASS2023-748

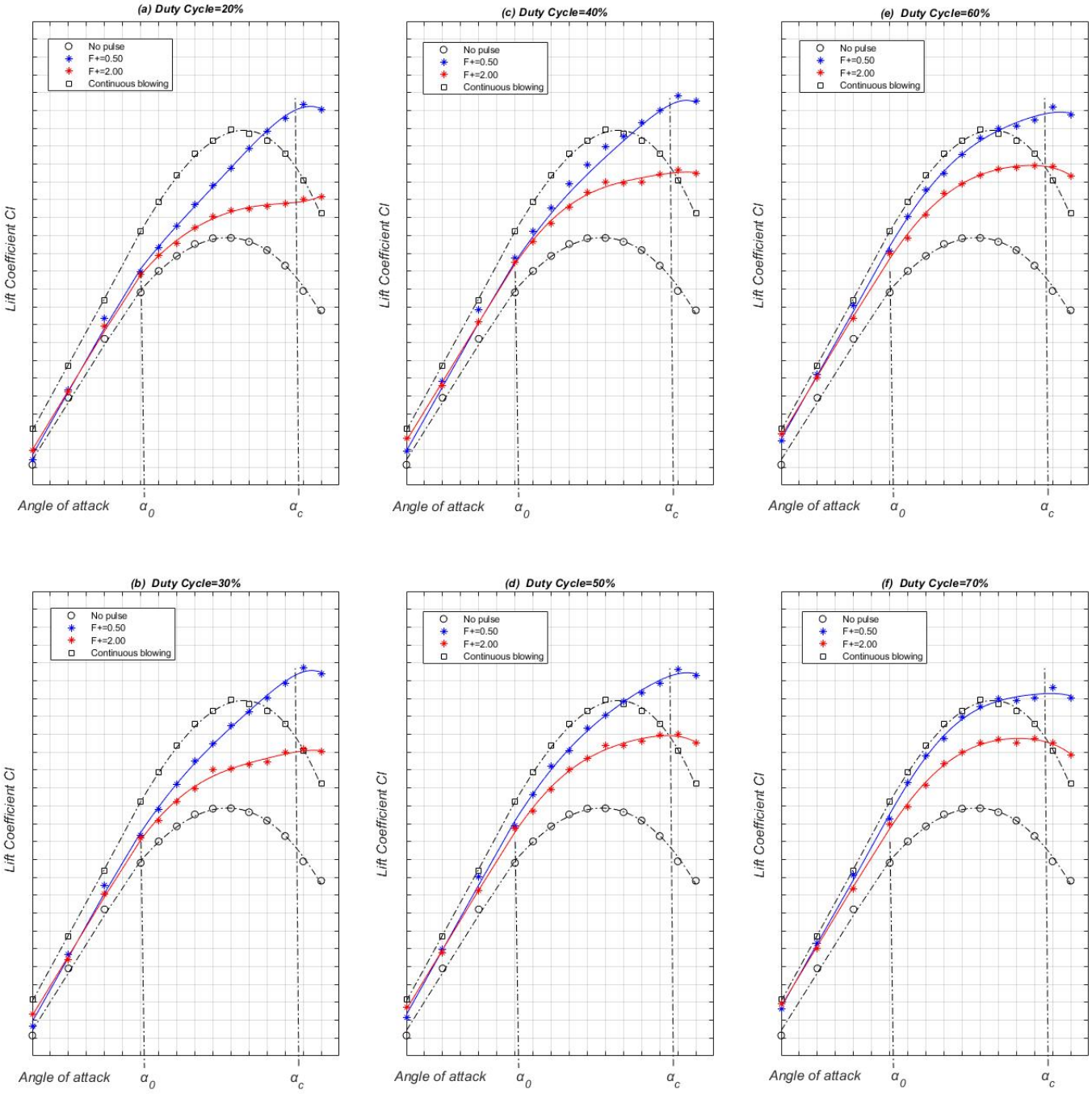

Fig. 8 Lift Coefficient at different DC: (a)=20%, (b)=30%, (c)= 40%, (d)=50%, (e)=60%, (f)=70%

Figure 9 shows how the jet velocity changed throughout the pulses. Figure 9 also demonstrates that at the frequency $F^+ = 0.5$, the jet velocities achieve their highest Mach number at low duty-cycle when compared to the high frequency $F^+ = 2.0$. Figure 9a demonstrates how, by preserving the pulse's square shape, the jet velocity appears to be responding quite remarkably to pulse actuation. It also demonstrates how the jet velocity peaks at the start of the pulse .Additionally, it demonstrates how the maximum jet velocity occurs at the start of the pulse and gradually decreases as the DC rises. However, when the duty cycle grows and the frequency rises to $F^+ = 2.0$, the velocity begins to lose its square form and sharp response. For almost all duty cycles, it only reaches a lower Mach number of $Ma \approx 0.8$.

Figure. 10 illustrates how the mass flow rate varies for various momentum coefficients C_μ and all the duty cycles. In this investigation the momentum coefficient $C_\mu = 0.0589$ is based on the jet velocity of continuous blowing. Figure. 10 also demonstrates that the PJA will use a mass-flow rate of around 11 grams/sec when pulsing at $DC = 20\%$ and at $F^+ = 0.5$. However, pulsing at $DC = 70\%$ and at $F^+ = 2.0$ the PJA requires as much as 34 gram/sec, which results in a

DOI: 10.13009/EUCASS2023-748

mass-flow rate differential of around 23 gram/sec. When these facts are compared to the data in Figure. 8, it becomes clear that low frequency and low duty cycle not only reduce mass-flow-rate but also drastically increase lift.

The pressure coefficient C_p distributions over the wing-model surface at the incidence α_2 with and without control are shown in Figure. 11. Likewise, the baseline pressure coefficients C_p for no control and continuous blowing are presented in Figure. 11a. It shows that the continuous blowing accelerates the flow over the main-wing-element and generates more lift along the 20-30% of the wing-model's chord C. Surprisingly, Figure. 11a also shows that the accelerated flow from the continuous blowing still accelerating the flow over the upper surface of the flap as well.

Comparison between the effect of the frequencies $F^+ = 0.5$ and $F^+ = 2.0$ at a fixed duty-cycle of 20%, is presented in Figure. 11b. It is noticeable that pulsing at a low frequency has more favourable effect than at a higher frequency. Pulsing at low frequencies and at 20% duty-cycle seems to maintain the flow over the wing-model highly accelerated for about 25% chord C and progressively decelerated to reach its initial state over the 60% of chord C. Pulsing at the high duty-cycle of 70% with both frequencies is illustrated in Figure. 11c. It shows that the duty-cycle of 70% seems to have shortened the effect of the pulsing. The high accelerated flow lasts only about 15% chord compared to a low duty-cycle and completely disappears at 45-50% chord.

Conclusion

An experimental investigation of pulsed jet actuator (PJA) flow separation control implemented in a three-element DLR F-15 wing in high-lift configuration is presented. The study focused on the control of the separation developed after the slat cutout at high angle of attack. Results show that the lift coefficient increases dramatically with different duty-cycles at low frequency $F^+ = 0.5$. Also, the stall angle α is delayed by 4°. The high frequency $F^+ = 2.0$ shows that the lift is always encapsulated between the baselines of no control and continuous blowing. It is suggested that the increase of the frequency will only bring the lift to the upper curve of continuous blowing.

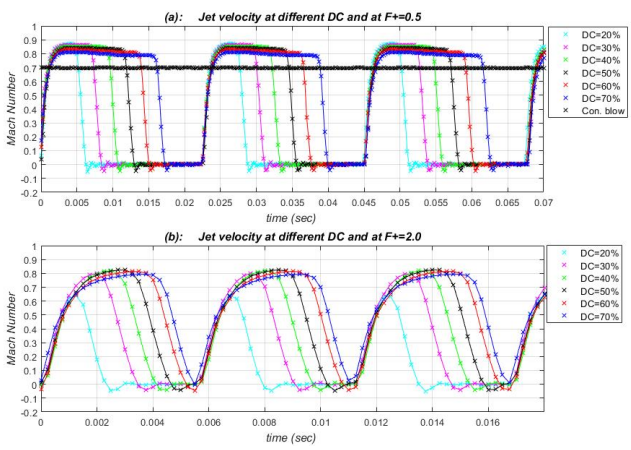

Fig. 9 Jet velocity at the exit of the nozzle Re=0.7 10^6

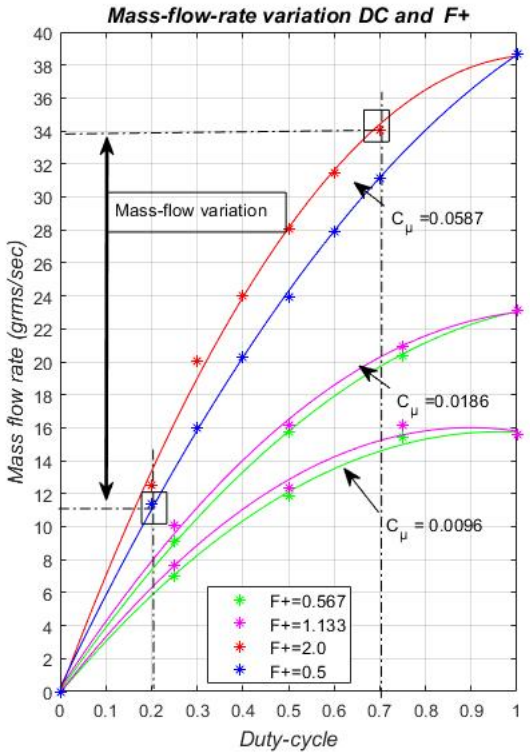

Fig. 10 Mass-flow-rate variation with $F^+ = 0.5$, $F^+ = 2.0$ along with the DC compared to other experiment cases

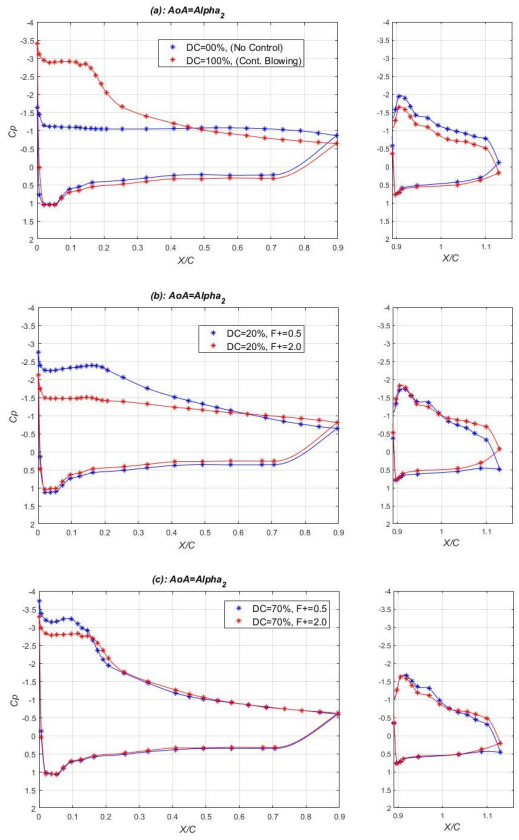

Fig. 11 C_p distribution across the wing model. Re=0.7 10^6, a:(DC=0% and 100%), b:(DC=20%, $F^+ = 0.5$,$F^+ = 2.0$), c:(DC=70%, $F^+ = 0.5$,$F^+ = 2.0$)

DOI: 10.13009/EUCASS2023-748

Acknowledgments

The work described in this paper has received funding from the European Community's Seventh Framework Program FP7/2020-2023, under the grant agreement no. 807792, WINGPULSE project.

References

[1] Ciobaca, V., and Wild, J., "An overview of recent DLR contributions on active flow-separation control studies for high-lift configurations," *AerospaceLab Journal*, , No. 6, 2013, pp. 1–12.

[2] Brunrt, V., Dandois, J., and Verbeke, C., "Recent Onera Flow Control Research on High-Lift Configurations," *AerospaceLab Journal*, , No. 6, 2013, pp. 1–12.

[3] Corke, T. C., Enloe, C. L., and Wilkinson, S. P., "Dielectric Barrier Discharge Plasma Actuators for Flow Control," *Annual Review of Fluid Mechanics*, Vol. 42, No. 24, 2010, pp. 505–529.

[4] Nishri, B., and Wygnanski, I. J., "Effects of Periodic Excitation on Turbulent Flow Separation from a Flap," *AIAA Journal*, Vol. 36, 1998, pp. 547–556.

[5] Ullah, J., Prachař, A., míd, M., Seifert, A., Soudakov, V. G., Lutz, T., and Krämer, E., "Reynolds number and wind tunnel wall effects on the flow field around a generic UHBR engine high-lift configuration," *CEAS Aeronautical Journal*, Vol. 11, 2020, pp. 1009 – 1023.

[6] Meyer, M., Lengers, M., Bieler, H., Fricke, S., Wild, J., and Norman, D., "Designing and Testing Active Flow Control Systems at the Junction of Ultra-High Bypass Ratio Engines and the Wing," *ECCOMAS presentation*, 2014.

[7] Ciobaca, V., Stefes, B., de Bruin, A., Bauer, M., Schlösser, P., de Blécourt, A., Bier, N., Zhai, J., Meyer, M., and Wild, J., "Wind tunnel experiment with local active flow control for aircraft towards future flight testing," *ICAS, 31st Cong. of the Int. Council of the Aeronautical Sciences*, 2018, pp. 1–16.

[8] Fricke, S., and Ciobaca, V., "Active Flow Control Applied at the Engine-Wing Junction," *CEAS Aeronautical Journal*, 2015, pp. 1–12.

[9] Schlösser, P., and Bauer, M., "Design of a pulsed jet actuator for separation control," *CEAS Aeronautical Journal*, Vol. 11, 2018, pp. 805 – 812.

[10] Lengers, M., "Industrial assessment of overall aircraft driven local active control," *29th Congress of the Internationalputer Council active fow control*, 2014.

[11] Cattafesta, L. N., and Sheplak, M., "Actuators for Active Flow Control," *Annual Review of Fluid Mechanics*, Vol. 43, 2011, pp. 247–272.

[12] Steinfurth, B., and Weiss, J., "Efficiency Enhancement in Active Separation Control Through Optimizing the Duty Cycle of Pulsed Jets," *AIAA Journal*, 2022.

[13] Hecklau, M., Salazar, D., and Nitsche, W. H., *Influence of the Actuator Jet Angle on the Reattachment Process with Pulsed Excitation*, Springer Verlag, 2013.

[14] Seifert, A., Darabi, A., and Wygnanski, I. J., "Delay of Airfoil Stall by Periodic Excitation," *Journal of Aircraft*, Vol. 33, 1996, pp. 691–698.

[15] Ciobaca, V., Kühn, T., Rudnik, R., Bauer, M., Gölling, B., and Breitenstein, W., "Active Flow-Separation Control on a High-Lift Wing-Body Configuration," *Journal of Aircraft*, Vol. 50, 2013, pp. 56–72.

[16] M. Jabbal, S. Z., "The near wall effect of synthetic jets in a boundary layer," *International Journal of Heat and Fluid Flow*, Vol. 29, 2008, pp. 119–130.

[17] Jabbal, M., Liddle, S. T., and Crowther, W. J., "Modelling the costs of implementing active flow control systems on civil transport aircraft," *KATnet II Conference on Key Aerodynamic Technologies, Bremen, Germany*, 2009.

[18] Jabbal, M., Liddle, S. T., and Crowther, W. J., "Active Flow Control Systems Architectures for Civil Transport Aircraft," *Journal of Aircraft*, Vol. 47, 2010, pp. 1966–1981.

[19] Schloesser, P., Soudakov, V. G., Bauer, M., and Wild, J., "Active Separation Control at the Pylon-Wing Junction of a Real-Scale Model," *AIAA Journal*, 2019.

[20] Stryczniewicz, W., Stalewski, W., Jabbal, M., and Bahri, F., "Development of Pulsed Jet Actuator for Power Efficient Actuation Concepts Testing," *AIAA AVIATION 2022 Forum*, 2022.

[21] Fricke, S., Ciobaca, V., Wild, J., and Norman, D., "Numerical Studies of Active Flow Control Applied at the Engine-Wing Junction," *Advances in Simulation of Wing and Nacelle Stall*, Vol. 131, Springer Verlag, 2014.